JACS
JOURNAL OF THE AMERICAN CHEMICAL SOCIETY

Article

pubs.acs.org/JACS

# Reactive Oxygen Species Mediated Activation of a Dormant Singlet Oxygen Photosensitizer: From Autocatalytic Singlet Oxygen Amplification to Chemicontrolled Photodynamic Therapy

Andrés M. Durantini,[†] Lana E. Greene,[†] Richard Lincoln,[†] Sol R. Martínez,[†,‡] and Gonzalo Cosa*[,†]

[†]Department of Chemistry and Center for Self-Assembled Chemical Structures (CSACS-CRMAA), McGill University, 801 Sherbrooke Street West, Montreal, Quebec H3A 0B8, Canada

[‡]Instituto Multidisciplinario de Biología Vegetal (IMBIV), CONICET, and Facultad de Ciencias Químicas, Universidad Nacional de Córdoba, Córdoba X5000HUA, Argentina

Supporting Information

**ABSTRACT:** Here we show the design, preparation, and characterization of a dormant singlet oxygen ($^1O_2$) photosensitizer that is activated upon its reaction with reactive oxygen species (ROS), including $^1O_2$ itself, in what constitutes an autocatalytic process. The compound is based on a two segment photosensitizer−trap molecule where the photosensitizer segment consists of a Br-substituted boron-dipyrromethene (BODIPY) dye. The trap segment consists of the chromanol ring of $\alpha$-tocopherol, the most potent naturally occurring lipid soluble antioxidant. Time-resolved absorption, fluorescence, and $^1O_2$ phosphorescence studies together with fluorescence and $^1O_2$ phosphorescence emission quantum yields collected on $Br_2B$−PMHC and related bromo and iodo-substituted BODIPY dyes show that the trap segment provides a total of three layers of intramolecular suppression of $^1O_2$ production. Oxidation of the trap segment with ROS restores the sensitizing properties of the photosensitizer segment resulting in ∼40-fold enhancement in $^1O_2$ production. The juxtaposed antioxidant (chromanol) and prooxidant (Br-BODIPY) antagonistic chemical activities of the two-segment compound enable the autocatalytic, and in general ROS-mediated, activation of $^1O_2$ sensitization providing a chemical cue for the spatiotemporal control of $^1O_2$.The usefulness of this approach to selectively photoactivate the production of singlet oxygen in ROS stressed vs regular cells was successfully tested via the photodynamic inactivation of a ROS stressed Gram negative *Escherichia coli* strain.

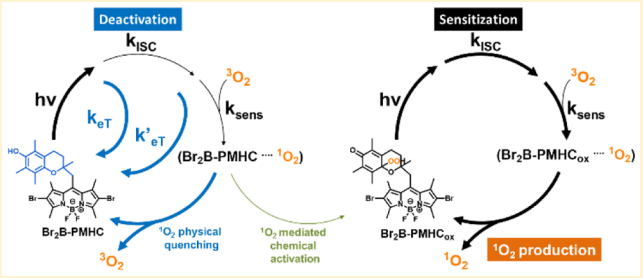


## INTRODUCTION

Photodynamic therapy (PDT) is a methodology used for the treatment of cancer and other ailments. It relies on the production of singlet oxygen ($^1O_2$), a reactive oxygen species (ROS) whose cytotoxic properties are exploited toward control of cell growth.[1−7] PDT requires for the interaction of light an active photosensitizer and molecular oxygen. Following excitation of the photosensitizer, rapid intersystem crossing (ISC) takes place from its singlet excited state to the triplet excited state. The triplet excited state next acts as an energy donor to ground state molecular oxygen ($^3O_2$) yielding $^1O_2$ generated *in situ*.[2,8−10]

In order to minimize undesired side effects, including damage to healthy tissue during PDT treatment, photosensitization of $^1O_2$ may be controlled at different levels. The specific targeting of the photosensitizer to ailing over healthy tissue and the precise delivery of the exciting light exclusively to the desired tissue constitute two levels of spatiotemporal control. Most recently the chemical activation of a photosensitizer specifically in the targeted tissue has emerged as an effective third level of control.[11−16] The method exploits differences in the proteome or metabolome of ailing tissue over the healthy tissue. An enzyme or a chemical agent prevailing in the targeted tissue may site-specifically activate an otherwise dormant chromophore into a potent photosensitizer.[12] Activation or unmasking of the otherwise dormant photosensitizer will occur upon, for example, the enzymatic hydrolysis of the quencher segment.[16]

We reasoned that a dormant singlet oxygen photosensitizer that activates upon scavenging of ROS could be utilized toward the controlled delivery of $^1O_2$ specifically in cells or tissues such as cancer cells that are under oxidative stress associated with increased metabolic activity and ROS generation.[17−21] Here we show the design of the compound $Br_2B$−PMHC that operates under this premise (see Scheme 1). The new compound is based on a two-segment photosensitizer−trap molecule. The photosensitizer segment consists of a Br substituted boron-dipyrromethene (BODIPY) dye, where substitution by heavy atoms ensures that rapid and efficient intersystem crossing to the triplet manifold will take place upon photoexcitation of the

**Received:** October 1, 2015
**Published:** January 20, 2016





DOI: 10.1021/jacs.5b10288
J. Am. Chem. Soc. 2016, 138, 1215−1225

**Scheme 1. Proposed Mechanism for Autocatalytic $^1O_2$ Amplification**[a]

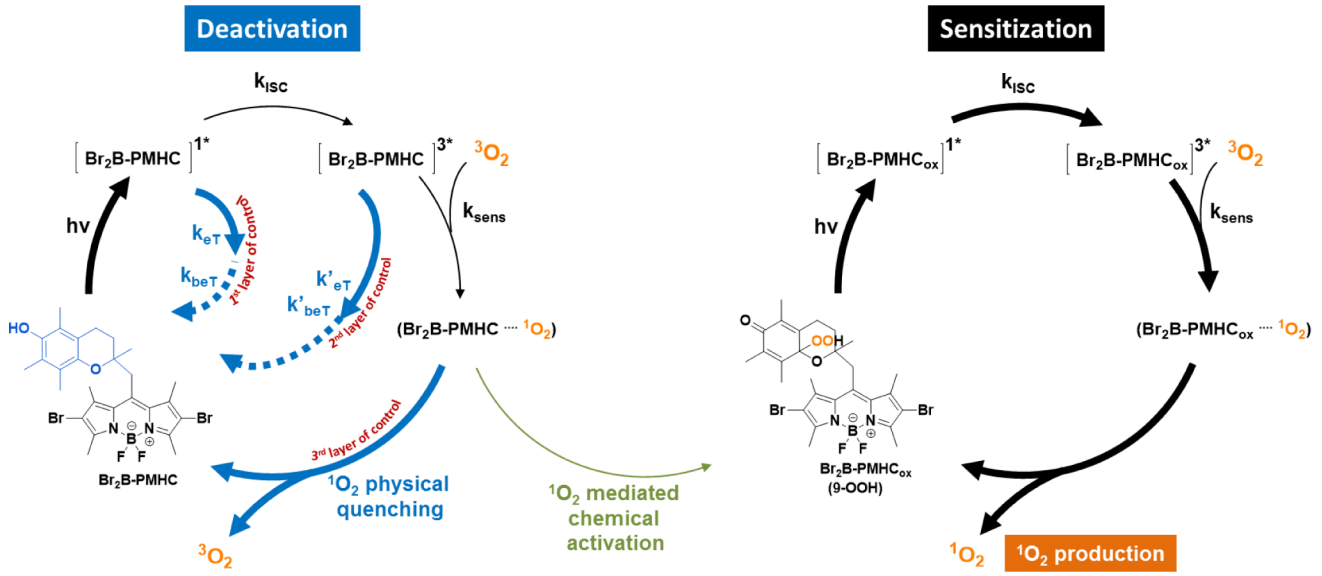


[a]Following photoexcitation of $Br_2B$–PMHC, its singlet excited state rapidly deactivates via intramolecular photoinduced electron transfer (PeT). PeT is also proposed to take place from the triplet excited state if at all formed. Any $Br_2B$–PMHC in the triplet manifold ($[Br_2B–PMHC]^3*$) that eludes the previous two decay pathways will sensitize $^1O_2$ that will next be scavenged through a physical process by the trap segment in $Br_2B$–PMHC (geminate reaction). The improbable occurrence of a chemical quenching pathway of $^1O_2$ by $Br_2B$–PMHC will yield an oxidized, active form, $Br_2B–PMHC_{ox}$, that will sensitize additional $^1O_2$.

chromophore.[8,13,22,23] The trap segment consists of the chromanol ring of $\alpha$-tocopherol, the most potent naturally occurring lipid soluble antioxidant and an efficient ROS scavenger.[24,25] Photoinduced electron transfer (PeT) from the chromanol segment to the BODIPY segment[26−31] is shown to effectively compete with intersystem crossing effectively reducing the yield of triplet state. Photoinduced electron transfer is also shown to quench any residual triplet excited state formed. Combined singlet and triplet quenching of the excited photosensitizer segment by the chromanol ring of $\alpha$-tocopherol is shown to give two layers of prevention of $^1O_2$ production. Importantly, $\alpha$-tocopherol, known to be an efficient physical quencher of $^1O_2$,[32−37] provides a third layer of suppression of $^1O_2$ production. Oxidation of the trap segment with ROS restores the ability of the compound to sensitize $^1O_2$ and aborts its ability to scavenge $^1O_2$ effectively activating the otherwise dormant photosensitizer (Scheme 1).The photophysical and reactivity studies described herein show that $Br_2B$–PMHC is a versatile ROS-activatable photosensitizer of potential application in tissues where metabolic imbalance leads to a large ROS production, such as in cancer cells[17−21] and wounded tissue.[38−40] The juxtaposed antioxidant-pro-oxidant antagonistic chemistry of $Br_2B$–PMHC enables the autocatalytic[41−44] ROS ($^1O_2$) amplification under continuous photoexcitation as ROS (including $^1O_2$) consumption triggers the photosensitization of $^1O_2$.

## RESULTS AND DISCUSSION

**Design and Preparation of an Activatable Photosensitizer.** We selected BODIPY dyes bearing heavy atoms such as I or Br at positions C2 and C6 for the photosensitizing segment (see Figure 1). First, BODIPY dyes are lipophilic, ensuring the partition of the new compound within the lipid membrane.[45,46] This partition enables rapid reaction of $^1O_2$ with unsaturated lipids, a target in PDT.[47−49] BODIPY dyes additionally have desirable spectroscopic properties including large extinction coefficients and small internal conversion decay rate constants, minimizing wasteful decay pathways.[50−53] BODIPY dyes are further relatively robust and inert toward $^1O_2$.[13] These dyes are easy to prepare and functionalize, enabling the substitution with halogens at positons C2 and C6 either before or after coupling the chromophore segment to the trap segment.[22,54,55] Decoration with either I or Br substituents ensures rapid ISC to the triplet manifold following photoexcitation of the chromophore.[13,22,55] Energy transfer from the BODIPY triplet excited state may then sensitize $^1O_2$. Finally, the redox potential of BODIPY dyes may be further tuned upon the judicious choice of substituents. Intramolecular PeT may then be implemented as a molecular switch to turn off/on a desired photophysical or photochemical outcome, for example, emission in fluorogenic probes[27−29,31,56] or $^1O_2$ sensitization, as shown in this work.

We reasoned that the chromanol moiety of $\alpha$-tocopherol was a most suitable trap segment to obtain a ROS activatable photosensitizer compound. First, and based on a correlation between Hammett parameters and BODIPY electrochemical potentials,[31] we estimated that rapid PeT from the chromanol segment to the excited singlet or triplet manifold of either a 2,6-dibromo- or a 2,6-diiodo-BODIPY photosensitizer segment would inactivate the sensitizing properties of the latter. Second, the electron rich chromanol ring is additionally an efficient $^1O_2$ quencher operating through both physical (93%) and chemical (7%) pathways.[34] The chromanol was thus expected to act as a molecular switch suppressing $^1O_2$ production at three different levels. Finally, oxidation of the chromanol following reaction with ROS would activate the photosensitizer as both PeT and $^1O_2$ scavenging processes are terminated (Scheme 1). Of note, our choice of chromanol coupled to a hydrophobic BODIPY dye ensured high specificity toward photosensitizer activation


DOI: 10.1021/jacs.5b10288
J. Am. Chem. Soc. 2016, 138, 1215−1225

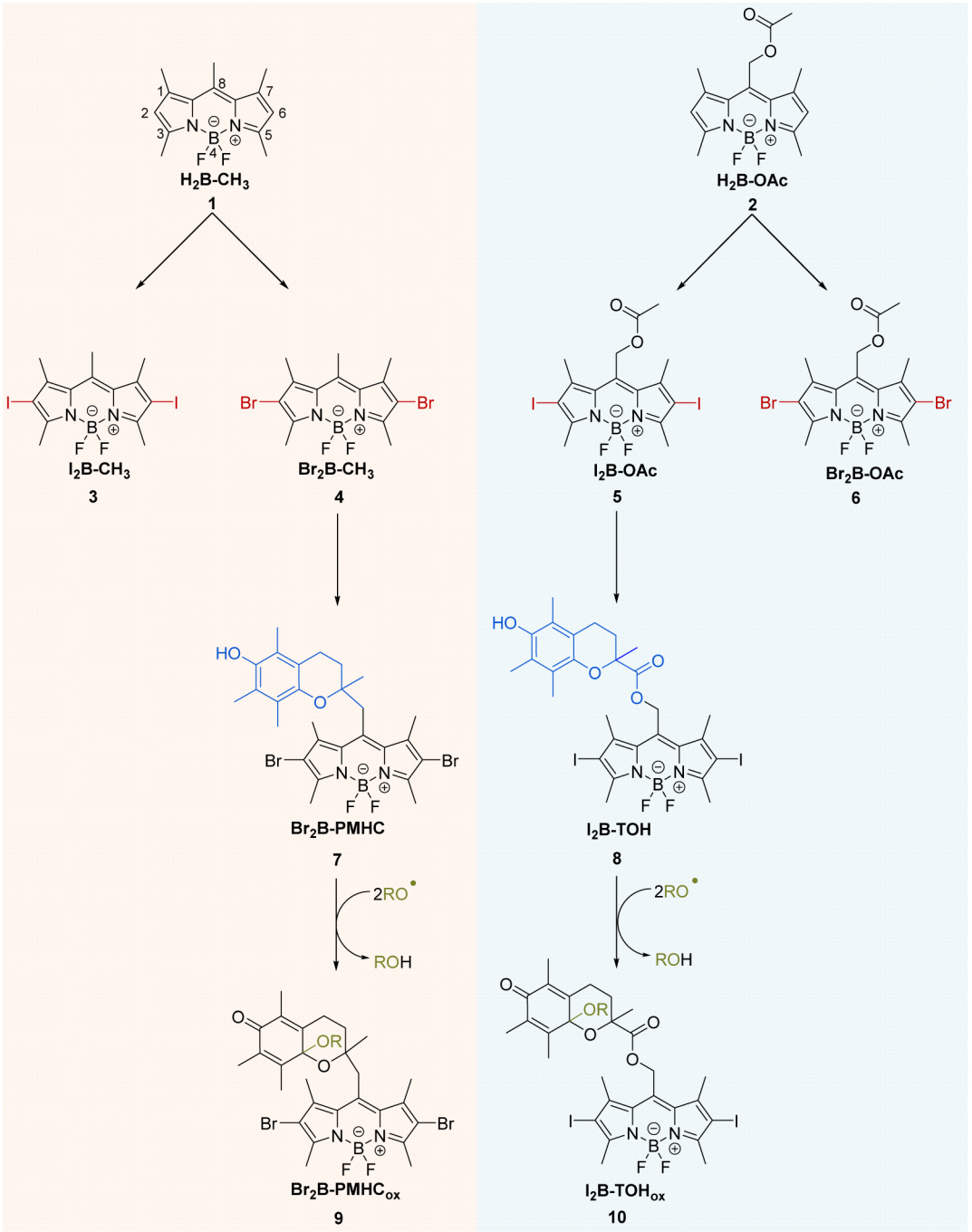


**Figure 1.** Compounds prepared and studied in this work. Compounds **1** and **2** are fluorescent controls for compounds **3** and **4** and **5** and **6**, respectively. Compounds **3** and **4** and **5** and **6** are photosensitizer controls for compounds **7** and **8**, respectively.

by lipid peroxyl radicals, the dominant ROS species encountered in lipid membranes under oxidative stress.[25,57−60]

We considered two different short linkers to connect the trap and photosensitizer segments.[29] One linker was based on a methylene linker connecting the chromanol and BODIPY moieties. An alternative strategy rested on an ester coupling, providing for a relatively simple synthetic route albeit in detriment of antioxidant activity as a result of the electron withdrawing effect on the chromanol trap of the carbonyl moiety.[29] Two compounds (**7** and **8**) were conceived bearing either Br or I, respectively, at positions C2 and C6 and a linker based on a methylene (**7**) vs an ester (**8**) moiety (Figure 1). Fluorescent control BODIPY dyes bearing either an ester or a methylene moiety and no halogen (**1** and **2**, Figure 1) and BODIPY dyes undergoing ISC but no PeT (controls bearing two Br or two I substitutions with either a methylene or an ester moiety yet lacking the chromanol segment) were also prepared and studied (compounds **3**−**6**, Figure 1).

$H_2B-CH_3$ (compound **1**) and $H_2B-OAc$ (compound **2**) were synthesized from the condensation of 2,4-dimethylpyrrole with acetyl or acetoxyacetyl chloride.[54] Halogenation of **1** and **2** via electrophilic aromatic substitution was used to introduce either I or Br specifically at positions C2 and C6 of the BODIPY. These positions are most susceptible to electrophilic attack given the electronic density of the BODIPY core.[50] We modified literature procedures[22] to introduce I, obtaining $I_2B-$



DOI: 10.1021/jacs.5b10288
J. Am. Chem. Soc. 2016, 138, 1215−1225

Table 1. Photophysical Properties of Compounds 1−8 in Acetonitrile at Room Temperature

| | $k_{dec} \times 10^7$ ($s^{-1}$)[b] | $k_{rad} \times 10^7$ ($s^{-1}$) | $k_{nr} \times 10^7$ ($s^{-1}$) | $\varepsilon \times 10^3$ ($M^{-1}$ $cm^{-1}$) | $\Phi_f$[a] | abs $\lambda_{max}$ (nm) | em $\lambda_{max}$ (nm) |
|---|---|---|---|---|---|---|---|
| 1[c] | 17.8 ± 0.1 | 14.4 ± 0.1 | 3.3 ± 0.1 | 97 | 0.81 ± 0.02 | 491 | 498 |
| 2[c] | 15.0 ± 0.2 | 13.1 ± 0.2 | 2.0 ± 0.1 | 81 | 0.87 ± 0.02 | 515 | 530 |
| 3 | 476.2 ± 0.7 | 13.1 ± 0.2 | 463.0 ± 0.7 | 83 | 0.03 ± 0.01 | 521 | 545 |
| 4 | 55.3 ± 0.2 | 11.0 ± 0.2 | 44.2 ± 0.2 | 79 | 0.20 ± 0.02 | 515 | 535 |
| 5 | 625.0 ± 0.7 | 12.5 ± 0.2 | 582.0 ± 0.7 | 96 | 0.02 ± 0.01 | 550 | 572 |
| 6 | 66.7 ± 0.3 | 9.3 ± 0.1 | 57.4 ± 0.2 | 81 | 0.14 ± 0.02 | 543 | 562 |
| 7 | d | d | d | 56 | ≤0.008 | 532 | 557 |
| 8 | 555.6 ± 0.6 | 5.0 ± 0.1 | 551.0 ± 0.5 | 63 | 0.009 ± 0.002 | 552 | 576 |

[a]Errors from duplicate experiments. [b]Fitting errors reported. [c]Values obtained from ref 31. [d]Not applicable.

$CH_3$ (compound **3**) and $I_2B$−OAc (compound **5**) in 72% and 79% yield, respectively, upon reaction of their respective precursors **1** and **2** with $I_2$ and $HIO_3$. $Br_2B$−$CH_3$ (compound **4**) and $Br_2B$−OAc (compound **6**) where obtained in 84% and 82% yield, respectively, upon direct halogenation of **1** or **2** using a slow addition of $Br_2$. $Br_2B$−PMHC (compound **7**) was obtained in 15% yield from the carefully controlled addition of $Br_2$ to our previously prepared $H_2B$−PMHC. $I_2B$−TOH (compound **8**) was obtained by coupling trolox to the halogenated BODIPY alcohol via a Mitsunobu reaction yielding the desired compound in 60% yield (since the newly formed compound **5** did not undergo hydrolysis under standard conditions, we hydrolyzed **2** and next halogenated the resulting alcohol following the procedure described above).

**Photophysical Studies.** In order to evaluate the rate of ISC, we initially compared the fluorescence parameters recorded for compounds **3** and **4** and **5** and **6**, bearing Br and I atoms, with those recorded for their unsubstituted fluorescent analogues **1** and **2**, respectively.

Table 1 lists the emission quantum yields ($\phi_f$) and the fluorescence decay rate constants ($k_{dec}$) recorded for compounds **1**−**8**. A 27-fold drop in $\phi_f$ was recorded following inclusion of I atoms in compound **1** (compare values for **1** and **3**). A ca. 44-fold drop was recorded when comparing **2** and its I-substituted analogue **5**. When BODIPYs were substituted with Br rather than I, smaller drops in $\phi_f$, ∼4-fold, were recorded in going from **1** to **4** and ∼6-fold in going from **2** to **6**. The drop in $\phi_f$, and concomitant increase in $k_{dec}$, can be attributed to the heavy atom effect that facilitates ISC processes.[13,22,61−65] The drop underscores the potential of these halogenated BODIPYs to be used as photosensitizer segments. Also listed in Table 1 are the values for the radiative rate constant estimated ($k_{rad} = \phi_f k_{dec}$) for compounds **1**−**8**. The values are consistent with those expected for the BODIPY core, in the range of $10 \times 10^7$ $s^{-1}$. Values for the decay rate constant associated with nonradiative processes were also estimated ($k_{nr} = (1 - \phi_f)k_{dec}$) and are likewise listed in Table 1. We recorded a 1 order of magnitude and 2 orders of magnitude increase in $k_{nr}$ upon substituting the parent BODIPY compound with Br and I, respectively (compare compound **1** with **3** and **4** and compound **2** with **5** and **6**). The increase in $k_{nr}$ in going from **1** or **2** to **3**−**6** may be safely assigned to the addition of a new decay pathway relying on ISC. Given the negligible contribution of $k_{nr}$ to the decay of **1** and **2**, one may then assign the measured values of $k_{nr}$ for compounds **3**−**6** to $k_{ISC}$. ISC is significantly more pronounced for iodo-bearing BODIPY dyes than for their brominated counterparts, resulting in $k_{ISC}$ being 1 order of magnitude larger for the former than for the later (iodo vs bromo).

Table 1 further lists the absorption and emission maxima and extinction coefficients for the new compounds (see also Figure 2). All of the dyes showed strong absorption bands between

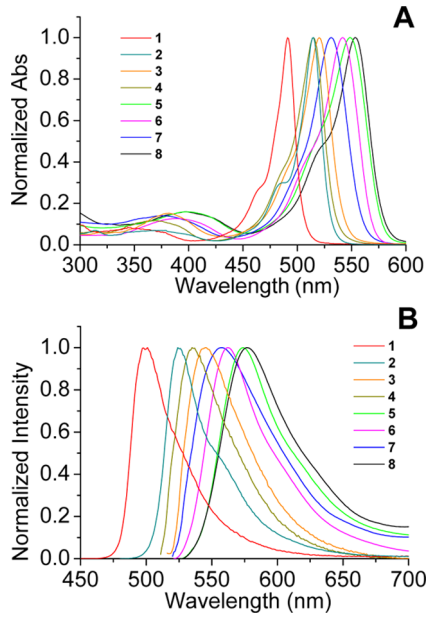


**Figure 2.** (A) Normalized absorption spectra and (B) normalized fluorescence emission spectra of compounds **1**−**8** in acetonitrile. Fluorescence spectra were obtained by exciting each compound at the first vibronic shoulder of the $S_0$−$S_1$ transition.

490 and 555 nm. Consistent with the stabilizing effect that electron withdrawing groups in the *meso* position have on BODIPY in its first excited singlet state,[66] a red shift in absorption and emission is observed in going from a methylene moiety to an acetate moiety (e.g., compare **1** vs **2**, **3** vs **5**, or **4** vs **6**) at the *meso* position. I- or Br-substitution also resulted in a bathochromic shift in the absorbance and emission spectra, indicating that the resonance donating effect of I and Br at positions C2 and C6 of the BODIPY core dominate over the inductive effect, where the effect is more pronounced for I than Br (compare **1** with **3** and **4** and **2** with **5** and **6**).

Consistent with intersystem crossing taking place in compounds **3**−**6**, nanosecond laser flash photolysis (LFP)[67] studies on these compounds showed the appearance of a long-lived transient species that was not detected with either control compound **1** or **2** (see Figure 3 and also Figure S1). The transient spectra were assigned to the triplet−triplet (T−T) absorption of compounds **3**−**6**.[68−70]Two peaks were observed in the regions between 420 and 440 and 600 and 700 nm. A negative band was also observed in the range from 460 to 570


DOI: 10.1021/jacs.5b10288
J. Am. Chem. Soc. 2016, 138, 1215−1225

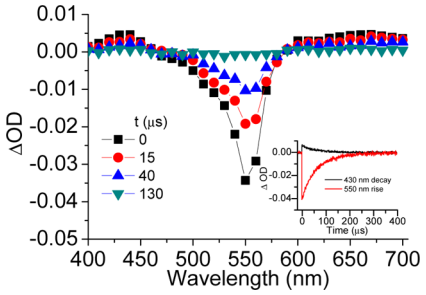


**Figure 3.** Transient absorption spectra of compound **5** in Ar saturated acetonitrile upon 532 nm laser excitation. The inset shows the time profile for ΔOD recorded at 430 and 550 nm.

nm, corresponding to the depletion of ground state BODIPY. Triplet decay rate constant $k_T$ values of $1.7 \times 10^4$ $s^{-1}$ and $2.7 \times 10^4$ $s^{-1}$ were recorded for the iodo-substituted BODIPYs (compounds **3** and **5**) and their bromo-substituted analogues (**4** and **6**), respectively, upon monitoring the T−T absorption time profile at either 430 nm or 550 nm in argon saturated solutions (see also Table 2). Consistent with the triplet assignment, the transients were readily quenched by molecular oxygen with quenching rate constant ($k_q$) values in the range of $(2-3) \times 10^9$ $M^{-1}$ $s^{-1}$, 1 order of magnitude smaller than the diffusion controlled rate constant in acetonitrile (Table 2).

**Control Layer for $^1O_2$ Production.** We subsequently tested via steady-state and time-resolved emission and LFP studies the extent to which the trap segment deactivates the production of $^1O_2$.

A first layer of control at the level of the singlet excited state was confirmed by the significant intramolecular quenching of fluorescence by the trap segment (Table 1).

Thus, for compound **7** (methylene linker), we recorded a ca. 25-fold drop in $\phi_f$ compared with the reference compound **4**. A ca. 2-fold drop in $\phi_f$ was recorded for **8** compared with **5**. The larger fluorescence sensitivity to insertion of the chromanol moiety recorded for **7** vs **8** arises from the slower rate of ISC and the faster rate of competing PeT for **7** (Br−BODIPY bearing a methylene linker) vs **8** (see also Table 1 for ISC and Table 3 and text below for PeT). Essentially, $k_{dec}$ for the control compound **5** is an order of magnitude larger than that for control **4**, and a new deactivation pathway (PeT in **8**) results in little changes to $\phi_f$ in going from **5** to **8**. Ultimately, the intramolecular switch introduced by the trap segment offers a better control and prevention of $^1O_2$ sensitization in **7** than **8**. Importantly, the measured fluorescence decays were too fast for **7** and **8** to obtain a reliable value for $k_{dec}$ in our setup. Based however on the $\phi_f$ value recorded for **7**, $\phi_f \leq 0.008$, we may safely place the value for the intramolecular electron transfer rate constant from the singlet state ($k_{eT}$) in compound **7** at $k_{eT} \geq 1 \times 10^{10}$ $s^{-1}$.

Consistent with quenching of the singlet via PeT from the chromanol segment, the Gibbs free energy for photoinduced electron transfer ($\Delta G^\circ_{eT}$) was exergonic for compounds **7** and **8**, in the range of 0.4 eV (see Table 3). This parameter was calculated based on eq 1,[8,71] utilizing the first singlet excited state energies and electrochemical redox potentials for compounds **1**−**6** listed in Table 3 (see Figure S2 for cyclic voltammograms).

$$\Delta G^\circ_{eT} = [e(E^\circ_{D^+\bullet/D} - E^\circ_{A/A^-\bullet}) + \omega - \Delta E_{00} \quad (1)$$

where $e$ is the elementary charge, $\omega$ is the electrostatic work term that accounts for the effect of Coulombic interaction of the radical ions formed upon reduction/oxidation, $\Delta E_{00}$ is the vibrational zero electronic energy of the excited fluorophore (either singlet or triplet), $E^\circ_{A/A^-\bullet}$ is the one-electron redox potential for the electron acceptor (BODIPY), and $E^\circ_{D^+\bullet/D}$ is the one-electron redox potential for the electron donor (phenol).

A second layer of control was subsequently tested via LFP studies, to monitor the extent to which the trap segment deactivates the triplet excited state of the photosensitizer. Intermolecular triplet quenching studies were conducted monitoring the decay of the T−T absorbance of compounds **3**−**6** at 430 nm in the presence of increasing concentrations of either 2,2,5,7,8-pentamethyl-6-hydroxy-chroman (PMHC, see Figure S3) or 6-hydroxy-2,5,7,8-tetramethylchromane-2-carboxylic acid (trolox). The two quenchers emulate the trap segments utilized in **7** and **8**, respectively. Quenching rate constant, $k_q$, values on the order of $1 \times 10^8$ to $4 \times 10^8$ $M^{-1}$ $s^{-1}$ were obtained for PMHC and compounds **3**−**6** (see also Table 2); no quenching was observed however for trolox, a chromanol like PMHC but bearing an electron withdrawing ester group and characterized by having a slightly higher oxidation potential than PMHC.

The intramolecular PeT quenching of the triplet excited state by the trap segment was next evaluated. Upon covalent attachment of the chromanol moiety to the photosensitizers (compounds **7** and **8**), a significant increase in the value of $k_T$ was observed. Specifically a 6-fold increase was observed for **8** compared with its precursor **5** (Table 2) revealing a moderate quenching by an ester linked chromanol segment. In the case of **7**, we were unable to detect any triplet−triplet absorption in

**Table 2. Triplet Excited State Properties and Singlet Oxygen Quantum Yields for Compounds 3−10 in Acetonitrile**

| | $k_T \times 10^4$ ($s^{-1}$), argon-purged | $k_T \times 10^6$ ($s^{-1}$) air-equilibrated | $k_q \times 10^9$[a] ($M^{-1}$ $s^{-1}$), Q = $^3O_2$ | $k_q \times 10^8$ ($M^{-1}$ $s^{-1}$), Q = PMHC | $\Phi_\Delta$[b] | $\Phi_\Delta$[c] |
|---|---|---|---|---|---|---|
| **3** | 1.68 ± 0.02 | 4.35 ± 0.02 | 1.82 ± 0.03 | 1.20 ± 0.05 | 0.75 ± 0.04 | 0.81 ± 0.02 |
| **4** | 2.70 ± 0.02 | 4.55 ± 0.03 | 1.91 ± 0.02 | 1.29 ± 0.04 | 0.64 ± 0.03 | 0.72 ± 0.02 |
| **5** | 1.64 ± 0.02 | 7.14 ± 0.04 | 3.01 ± 0.01 | 3.95 ± 0.07 | 0.95 ± 0.03 | 0.98 ± 0.03 |
| **6** | 2.72 ± 0.03 | 6.67 ± 0.04 | 2.80 ± 0.02 | 2.23 ± 0.05 | 0.79 ± 0.02 | 0.84 ± 0.02 |
| **7** | *d* | *d* | *d* | *d* | *d* | *d* |
| **8** | 9.16 ± 0.05 | 4.55 ± 0.02 | 1.88 ± 0.02 | 5.90 ± 0.09 | 0.46 ± 0.03 | 0.57 ± 0.02 |
| **9** | 3.12 ± 0.02 | *d* | *d* | *d* | 0.57 ± 0.03 | 0.68 ± 0.02 |
| **10** | 1.58 ± 0.02 | *d* | *d* | *d* | 0.87 ± 0.02 | 0.92 ± 0.03 |

[a]Values calculated considering that the solubility of oxygen in acetonitrile is 2.42 mM according to ref 72. [b]Singlet oxygen quantum yields calculated from the consumption of dimethylanthracene using Rose Bengal as a standard, $\Phi_\Delta$(RB) = 0.54,[73] $k^{DMA}_{obs} = 6.3 \times 10^{-3}$ ($s^{-1}$). [c]Singlet oxygen quantum yield determined directly from phosphorescence studies. Data were represented as the mean ± standard deviation of each group. [d]Not applicable.



DOI: 10.1021/jacs.5b10288
J. Am. Chem. Soc. 2016, 138, 1215−1225

**Table 3. Electrochemical Data, HOMO and LUMO Orbital Energies, Singlet Excited State and Triplet Excited State Energies, and Gibbs Free Energies for PeT**

| | $E_{00}$[a] (eV) | $E$(triplet)[b] | $\varepsilon_{LUMO}$[c] (eV) | $\varepsilon_{HOMO}$[d] (eV) | $E^{\circ}_{B^{+\bullet}/B}$[e] | $E^{\circ}_{pc}$[f] | $\Delta G_{eT}$ (singlet) | $\Delta G_{eT}$ (triplet) |
|---|---|---|---|---|---|---|---|---|
| **1**[g] | 2.53 | *i* | −2.31 ± 0.05 | −5.36 ± 0.01 | 0.77 | *i* | −0.26 | *i* |
| **2**[h] | 2.38 | *i* | −2.61 ± 0.05 | −5.49 ± 0.01 | 0.75 | −1.44 | −0.24 | *i* |
| **3** | 2.33 | 1.70 | −2.87 ± 0.05 | −5.81 ± 0.01 | 0.88 | *i* | −0.37 | 0.262 |
| **4** | 2.37 | 1.71 | −2.94 ± 0.05 | −5.75 ± 0.01 | 0.89 | *i* | −0.38 | 0.282 |
| **5** | 2.21 | 1.54 | −3.09 ± 0.05 | −5.87 ± 0.01 | 0.91 | −1.14 | −0.4 | 0.269 |
| **6** | 2.25 | 1.53 | −3.15 ± 0.05 | −5.81 ± 0.01 | 0.94 | −1.13 | −0.43 | 0.287 |

[a]$E_{00}$ = HOMO−LUMO gap obtained from the intercept of the normalized absorption and emission spectra. [b]Energy of the lowest triplet state, from phosphorescence emission spectra. [c]Energy of the lowest unoccupied molecular orbital derived from Hammett constants and associated errors. [d]Energy of the highest occupied molecular orbital derived from Hammett constants and associated errors. [e]$E^{\circ}_{B^{+\bullet}/B}$ = reversible oxidation potential. [f]$E^{\circ}_{pc}$ = cathodic peak potential. [g]Values obtained from ref 54. [h]Values obtained from ref 31. [i]Not applicable.

contrast to its precursor **4**, signaling that little triplet was formed as a result of efficient PeT in the singlet excited state or signaling an extremely rapid intramolecular quenching of the triplet excited state from the methylene-linked chromanol trap segment via PeT (vide infra). The intramolecular PeT quenching is much faster for a chromanol lacking the ester moiety, consistent with the intermolecular quenching studies described above. The intramolecular triplet quenching in **7** and **8** thus provided a second layer of control on the photosensitizer activity, at the level of the precursor triplet state.

The value of $\Delta G^{\circ}_{et}$ for the first excited triplet state was calculated utilizing eq 1 and the triplet excited state energy obtained from phosphorescence emission of compounds **3**−**6** (see Table 3 and Figure S4). Based on these calculations $\Delta G^{\circ}_{et}$ for PeT from the chromanol to the triplet excited state of **3**−**6** was endergonic, ca. 0.27 eV, accounting for the small intermolecular rate constant of quenching measured for these compounds in the presence of either PMHC or trolox and for the long triplet decay rate constant $k_T$ recorded for compound **8**. Importantly, the efficiency of PeT also relies on the distance between the trap segment and the photosensitizers, a factor that may additionally contribute to the differences observed between compound **7** (methylene linker) and compound **8** (ester linker).

The third layer of control involving geminate quenching of $^1O_2$ by the trap segment was next explored. The chromanol ring in α-tocopherol is an efficient $^1O_2$ quencher[32−37,74] where mostly physical (93%) but also chemical (7%) deactivation takes place.[34,75] To test whether **7** is equally efficient at deactivating $^1O_2$ as α-tocopherol, we generated $^1O_2$ upon irradiation of compound **5** and monitored the $^1O_2$ phosphorescence lifetime in the presence of increasing amounts of either **7** or PMHC (an α-tocopherol analogue lacking the phytyl tail). We measured similar rate constants (see Figure 4) for the intermolecular quenching rate constants of $^1O_2$ by **7** and PMHC ($k_q$ = 2.0 × $10^8$ $M^{-1}$ $s^{-1}$ and $k_q$ = 4.0 × $10^8$ $M^{-1}$ $s^{-1}$, respectively) indicating that **7** is an efficient $^1O_2$ quencher, on par with α-tocopherol.

In order to quantify the quantum yield of singlet oxygen generation ($\Phi_\Delta$) for the control compounds **3**−**6**, the deactivated compounds **7** and **8**, and their activated forms **9** and **10** (*vide infra*), we measured the phosphorescence of $^1O_2$ at 1270 nm (direct method, Figure 5). An indirect method based on changes in the absorbance of 9,10-dimethylanthracene upon its oxidation by $^1O_2$ was also applied (see Figures S5 and S6).[76] In both cases, the $\Phi_\Delta$ from Rose Bengal was used as a reference.[73] Similar $\Phi_\Delta$ values were obtained for the

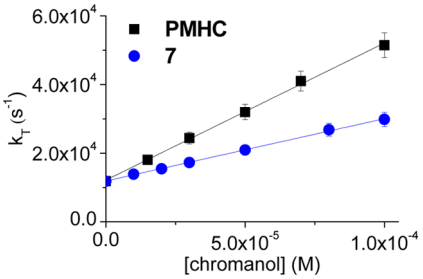


**Figure 4.** Decay rate constant for $^1O_2$ phosphorescence in the presence of increasing concentration of chromanol rings (either compound **7** or PMHC). $^1O_2$ was generated upon irradiation of compound **5** in air-equilibrated acetonitrile solutions. Values represent mean ± standard deviation of three separate experiments.

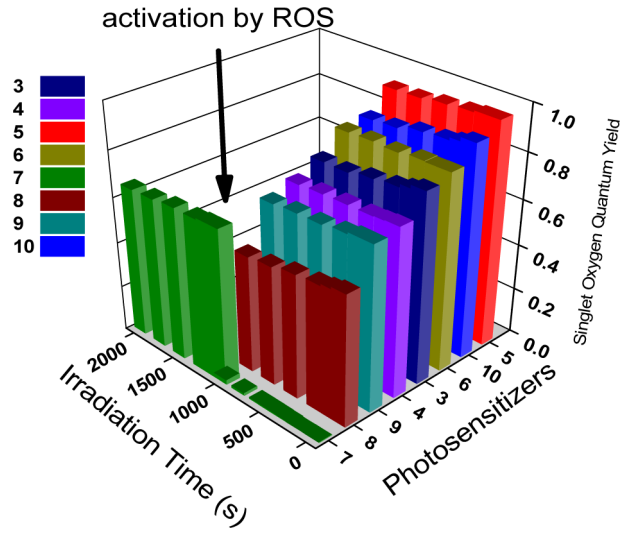


**Figure 5.** $^1O_2$ phosphorescence emission intensities ($\lambda_{em}$ = 1270 nm) as a function of irradiation time for the different photosensitizers in air-equilibrated acetonitrile solutions. Compound **7** was activated following reaction with cumyloxyl radicals. The solution of **7** contained an equimolar amount of sacrificial PMHC to prevent premature oxidation of **7**. A pulsed laser operating at a 10 Hz frequency and with a 532 nm output of 10 mJ/pulse was employed to excite the sample.

compounds under study using either the direct determination or the photooxidation of dimethylanthracene (see Table 2).

Iodo-substituted BODIPYs **3** and **5** showed comparable values of $\Phi_\Delta$ (0.81 and 0.98, respectively) roughly 10% larger than those of their brominated counterparts **4** and **6**, respectively. This is consistent with ISC being significantly


DOI: 10.1021/jacs.5b10288
J. Am. Chem. Soc. 2016, 138, 1215−1225

more pronounced for iodo-bearing BODIPY dyes than for their brominated counterparts. In general, the $\Phi_\Delta$ values for compounds **3**–**6** also correlate with ISC being the dominant decay pathway in the iodo- or bromo-substituted BODIPYs in comparison to their unsubstituted counterparts **1** and **2**. Addition of Br to the BODIPY core is shown to increase the overall singlet excited state decay rate constant, $k_{dec}$, in the range 3.1–4.5-fold (compare **1** vs **4** or **2** vs **6**), that is, ISC accounts for 2/3 to 4/5 of the overall singlet excited state deactivation. One may thus expect at best a 60%–80% value for $\Phi_\Delta$, consistent with the tabulated values in Table 2. In turn $k_{dec}$ increased ca. 27-fold and 42-fold upon iodo-substitution (compare **1** vs **3** or **2** vs **5**). In this case, $\Phi_\Delta$ is expected to be above 95%, as was observed for **5**. The slightly smaller $\Phi_\Delta$ recorded for **3** may be the result of $^1O_2$ quenching by the more nucleophilic BODIPY **3** lacking the ester group of **5**. In line with this argument, **3** was observed to photodegrade at a slightly larger pace than **5** presumably via photooxidation (see Figure 5).

We observed no $^1O_2$ generation for freshly prepared solutions of **7**. Geminate (static) quenching of $^1O_2$ in compound **8** by the chromanol trap segment was inferred from its $\Phi_\Delta$ value, which was ca. 1/2 that recorded for its control compound 5. This would be consistent with the third control layer of $^1O_2$.

**Activation of the Photosensitizer.** Activation of the dormant photosensitizer **7** or **8** (deactivation of PeT) following their reaction with ROS was subsequently tested in the presence of alkoxyl radicals. These ROS were generated at a constant rate upon photolysis at 263 nm of an air-equilibrated 100 $\mu$M dicumyl peroxide solution in acetonitrile. We followed over time the increase in fluorescence intensity (drop in PeT) to monitor the extent of activation, see Figure S7. Activation was complete once the intensity reached a plateau.[28,45] At this point, the trap segment in **7** and **8** reacted to completion with alkoxyl radicals to generate **9** and **10**, respectively. Consistent with deactivation of PeT in the triplet excited state following ROS scavenging by **7** and **8**, values of $k_T$ recorded with the oxidized compounds **9** and **10** were comparable to those obtained for control compounds **3**–**6** (see Table 2). Deactivation of PeT in the singlet excited state in turn manifested in the ca. 7-fold and 2-fold emission enhancements recorded for **9** vs **7** and **10** vs **8**, respectively (Figure S7).

Direct activation of **7** to yield **9** upon reaction with cumyloxyl radicals resulted in a dramatic increase in $^1O_2$ generation. We recorded a ca. 40-fold enhancement in $\Phi_\Delta^D$ for **9** with respect to **7** (Figure 4). The $\Phi_\Delta$ recorded for **9** is further comparable to the one achieved for the control compound **4**, indicating that the photosensitizing properties of the Br-substituted BODIPY were fully restored. Compounds **10** (activated **8**) and **5** had the same $\Phi_\Delta$. Importantly, we recorded a $^1O_2$ phosphorescence decay lifetime of ca. 80 $\mu$s upon photosensitization by all compounds but **7** (where $^1O_2$ was not generated) and by **8**, where the lifetime dropped to 70 $\mu$s, consistent with intermolecular quenching of $^1O_2$ by the chromanol moiety, that is, $^1O_2$ that was not scavenged by its source was eventually scavenged intermolecularly.

**Autocatalytic Activation and $^1O_2$ Amplification.** The juxtaposed antioxidant (chromanol) and prooxidant (Br–BODIPY) antagonistic chemical activities of the two-segment compound paved the way for the autocatalytic activation of $^1O_2$ sensitization (Scheme 1).[77] Photoexcitation of solutions containing trace impurities of oxidized **7** or direct excitation of **7** where the three control layers were avoided (see Scheme 1), resulted in the generation of initially undetectable amounts $^1O_2$ that were capable of reacting with the trap segment in **7**. Chemical rather than physical quenching of the trace amounts of $^1O_2$ by **7** yielded, we postulate, compound **9-OOH** (see Scheme 2), resulting in activation of otherwise dormant **7** and

**Scheme 2. Proposed Reaction of 7 with $^1O_2$**

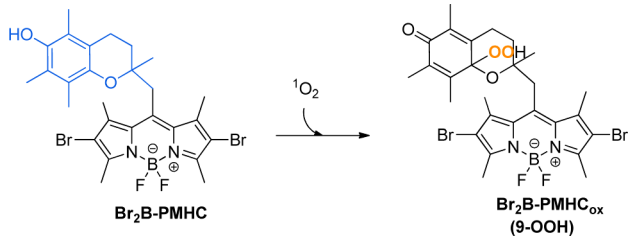


the amplification of $^1O_2$ generation. Consistent with an autocatalytic activation mechanism, the $\Phi_\Delta$ recorded following direct 532 nm laser excitation of an air-equilibrated acetonitrile solution of **7** was observed to increase over time following a sigmoidal behavior (Figure 6).[41−44] A ca. 6-fold increase in $\Phi_\Delta$

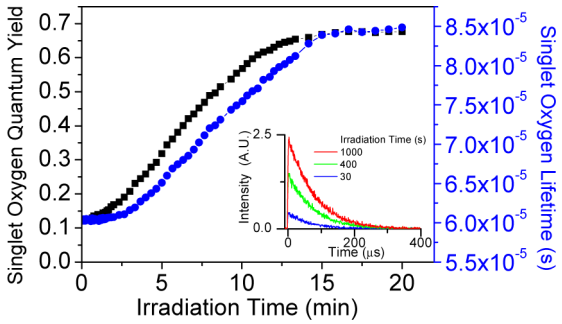


**Figure 6.** Singlet oxygen quantum yield (■) and singlet oxygen lifetime (●) for compound **7** as a function of the irradiation time. The inset shows $^1O_2$ phosphorescence decay traces recorded at 1270 nm following increasing irradiation times. [**7**] = 5.8 $\mu$M in air-equilibrated acetonitrile solutions. A pulsed laser operating at a 10 Hz frequency and with a 532 nm output of 10 mJ/pulse was employed to excite the sample.

was initially recorded. The $^1O_2$ phosphorescence lifetime also followed a similar sigmoidal behavior with irradiation time, increasing from ca. 60 to 85 $\mu$s. Both the sigmoidal increase in phosphorescence lifetime and in $\Phi_\Delta$ are consistent with depleting the trap segment in **7** thus reducing the amount of $^1O_2$ quencher while simultaneously yielding an active sensitizer, presumably compound **9-OOH**.

Intrigued by the relatively small enhancement in $\Phi_\Delta$ experimentally observed, we reasoned that some initial reaction may take place upon preparing solutions of **7**. Direct activation upon reaction with cumyloxyl radicals yielded 40-fold enhancement (Figure 5); however sacrificial amounts of PMHC (1 equiv of PMHC per equivalent of **7**) were added in that case to the solvent to prevent premature oxidation of **7**. We next monitored $\Phi_\Delta$ and $^1O_2$ phosphorescence decay upon adding 250 $\mu$M PMHC to the solution prior to addition of compound **7** (Figure S8). In this case, the $^1O_2$ phosphorescence lifetime was within the instrument response, that is, ~3 $\mu$s. The $\Phi_\Delta$ was further undetectable. Prolonged irradiation of this solution (8 h, ~300 000 laser shots, 10 mJ/pulse) resulted in a ca. 25-fold


DOI: 10.1021/jacs.5b10288
J. Am. Chem. Soc. 2016, 138, 1215–1225

increase in $\Phi_\Delta$. Importantly, photodegradation of the BODIPY chromophore presumably prevented reaching the maximum possible enhancement in this case.

While monitoring the increase of $^1O_2$ phosphorescence or lifetime gave a qualitative picture of the autocatalytic activation of **7**, we reasoned that monitoring fluorescence increase real-time would provide a means to better analyze the autocatalytic process. Although **7** is sparingly emissive ($\Phi_f \leq 0.008$), the activated form would have similar emission to that of control **4**, characterized by a $\Phi_f = 0.20$, thus enabling tracing the activation over time via the increase of fluorescence emission intensity. Continuous irradiation of an air-equilibrated solution of **7** in acetonitrile within a fluorimeter exciting at 532 nm displayed a sigmoidal enhancement in emission (see Figure 7

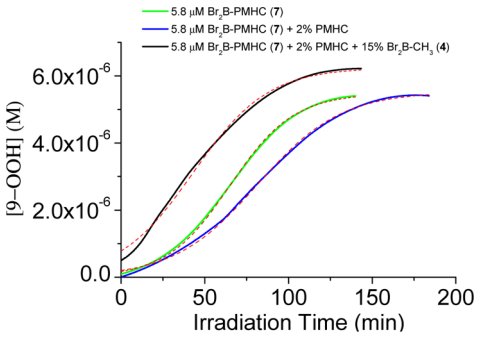


**Figure 7.** Autocatalytic activation of compound **7** to generate **9-OOH** as a function of irradiation time. Experiments were conducted in air-equilibrated solutions in acetonitrile containing 5.8 $\mu$M **7** (green trace), 5.8 $\mu$M **7** and 0.12 $\mu$M PMHC (2% equiv of **7**, blue trace), and 5.8 $\mu$M **7**, 0.12 $\mu$M PMHC, and 0.87 $\mu$M **4** (15% equiv of **7**, black trace). In this latter case please note that the trajectory considers **4** as a surrogate of activated compound **9-OOH**. Fitting of the data according to eq 4 are shown by the red dashed lines. The power of the incident light was 1.6 mW/cm$^2$.

and Figure S9 for the raw data).[41−44,78] In order to avoid the preoxidation of **7**, we next added 0.12 $\mu$M of sacrificial PMHC (2% equivalents of **7**) to the solvent. Fluorescence intensity enhancements of ∼30-fold were recorded in the latter case. This sample also displayed a longer induction period than that recorded when no PMHC was added. To emulate conditions of exacerbated preoxidation of **7**, we next conducted experiments where 0.87 $\mu$M of **4** were added to the solution (15% equiv of **7**). Compound **4** was utilized to correctly account for the amount of activated singlet oxygen sensitizer; it is thus a surrogate of compound **9**. In this case, no induction period was observed (Figures 7 and S9). The autocatalytic process (eq 2 below) under conditions of increasing amounts of activated compound follows the rate law given by eq 3, and the experimental results may be fitted according to eqs 4−7.[41]

$$\mathbf{7} \xrightarrow{k} \mathbf{9\text{-}OOH} \tag{2}$$

Given the above reaction scheme the rate equation becomes

$$\frac{-\mathrm{d}[\mathbf{7}]}{\mathrm{d}t} = k[\mathbf{7}][\mathbf{9\text{-}OOH}] = \frac{\mathrm{d}[\mathbf{9\text{-}OOH}]}{\mathrm{d}t} \tag{3}$$

The solutions for [**7**] and [**9-OOH**] given the autocatalytic process are given by

$$[\mathbf{9\text{-}OOH}] = [\mathbf{9\text{-}OOH}]_0 + \frac{b[\mathbf{7}]_0(\mathrm{e}^{at} - 1)}{1 + b\,\mathrm{e}^{at}} \tag{4}$$

$$[\mathbf{7}] = [\mathbf{7}]_0 - \frac{b[\mathbf{7}]_0(\mathrm{e}^{at} - 1)}{1 + b\,\mathrm{e}^{at}} \tag{5}$$

where $a$ and $b$ are given by

$$a = ([\mathbf{7}]_0 + [\mathbf{9\text{-}OOH}]_0)k \tag{6}$$

and

$$b = \frac{[\mathbf{9\text{-}OOH}]_0}{[\mathbf{7}]_0} \tag{7}$$

In eqs 2−7 $k$ is an apparent second order rate constant.[41] Doing a direct correlation between the fluorescence intensity and the initial concentration of **7** and assuming that all **7** is oxidized to yield **9-OOH**, it was possible to obtain the concentration vs time profile for the photooxidation of **7** (see Figures 7and S9). The data was fit according to eq4. The $k$ values retrieved for the autocatalytic activation of **7** under different conditions were on the order of $8.0 \times 10^3$ M$^{-1}$ min$^{-1}$. As previously described, less than 5% of **7** is preoxidized during the preparation of our sample. This value is consistent with the initial concentration of **9-OOH** obtained from the fitting of the trajectory acquired with **7** only (no PMHC or compound **4**).

**Photodynamic Inactivation of Bacteria.** We next validated the applicability of compound **7** toward the selective photodynamic inactivation of ROS-stressed vs regular bacteria. To stress the cells, we utilized hydrogen peroxide, known to stimulate ROS production in Gram-negative cells.[79,80] We incubated bacteria from the *Escherichia coli* strain ($10^6$ colony forming units (CFU)/mL) with 500 nM hydrogen peroxide for 2 h at 37 °C. Following precipitation and resuspension of this bacteria in media with no $H_2O_2$, we added compound **7**. In parallel, compound **7** was also added to bacteria that were not exposed to $H_2O_2$. We next tested the bactericidal capability of compound **7** in both the ROS stressed (*E. coli* (i) + **7**) vs regular cells (incubated with no $H_2O_2$ (*E. coli* + **7**)) by counting *E. coli* colony forming units remaining after 1 h of continuous irradiation (2.6 mW/cm$^2$ with a maxima at 520 and a fwhm of 31 nm for 5 lamps 10 cm from the target), see Figure 8.

A drastic drop in colony forming units was recorded following the combined action of compound **7** and irradiation for stressed cells. No inactivation was observed in turn for nonstressed healthy cells. A control experiment where cells were treated with preactivated **7** (compound **9**) and light but no $H_2O_2$ also showed a drastic drop in CFU. Additional control experiments in the dark for cells treated with compound **9** or with compound **7** (with or without $H_2O_2$), or simply with $H_2O_2$ showed no effect on the CFU, see Figure 8.

## ■ CONCLUSION

The juxtaposed antioxidant and prooxidant antagonistic chemical activities of the newly developed dormant photosensitizer $Br_2B$−PMHC (**7**) enable the autocatalytic, and in general ROS-mediated, activation of $^1O_2$ sensitization providing a chemical cue for the spatiotemporal control of $^1O_2$ production. Kinetic and spectroscopic considerations show that the faster rate of ISC recorded for iodo- vs bromo-substituted BODIPY segments, while desirable toward enhancing the yield of $^1O_2$ sensitization, provides a strain on the kinetic control of dormancy, that is, a faster ISC rate necessitates faster rates of photoinduced electron transfer in order for the photosensitizer to be effectively dormant. This is exemplified by comparing compounds **7** and **8**. Dormancy in


DOI: 10.1021/jacs.5b10288
J. Am. Chem. Soc. 2016, 138, 1215−1225

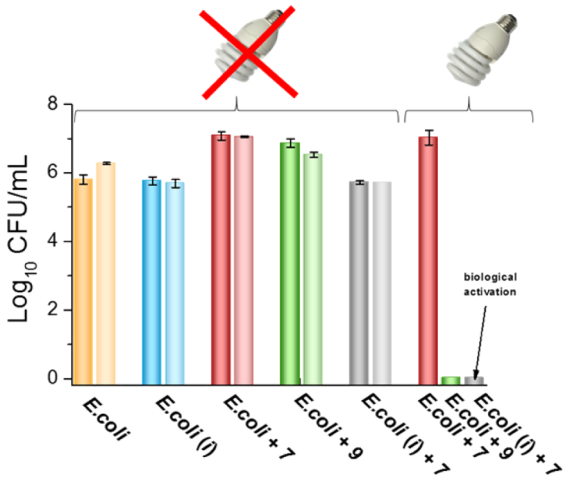


**Figure 8.** Antibacterial photodynamic inactivation in *E. coli* ATCC 25922. *E. coli* dark controls (from left to right): control, incubated with 500 nM hydrogen peroxide (i), treated with **7**, treated with **9**, incubated with 500 nM hydrogen peroxide and treated with **7**. *E. coli* after 1 h irradiation (from left to right): *E. coli* treated with **7**; *E. coli* treated with **9** (preactivated **7**), and *E. coli* incubated with 500 nM hydrogen peroxide and treated with **7**. Dimmer colors represent the strain treated for 1 h with compound **7** or **9** and intense colors indicates no incubation period with compound **7** or **9**.

the former results from a fast rate of PeT (methylene-linked chromanol) and a moderately large rate of ISC (bromo-bearing compound), whereas in the latter, characterized by a smaller rate of PeT (ester-linked chromanol) and a larger rate of ISC (iodo-bearing compound), dormancy is not achieved. From a spectroscopic viewpoint, the moderately large rate of ISC observed in bromo-substituted BODIPY dyes results in residual emission ($\Phi_f \approx 15\%$) being observed from these compounds, enabling real-time monitoring of the activation of the dormant photosensitizer bearing Br atoms, which will be of particular significance in cell studies. This does not come in major detriment of the quantum yield of $^1O_2$ for the Br-bearing BODIPY, at ca. 80%. Compound **7** provides a new paradigm toward developing photosensitizers that will enable the controlled delivery of $^1O_2$ specifically in cells or tissues where metabolic imbalance leads to a large production of ROS, acting as a trigger and amplifier for $^1O_2$ photosensitization. The usefulness of this approach to selectively photoactivate the production of singlet oxygen in ROS stressed vs regular cells was successfully tested via the photodynamic inactivation of a ROS stressed Gram negative *E. coli* strain.

## EXPERIMENTAL SECTION

**Materials.** HPLC grade solvents for spectroscopy experiments and column chromatography purifications, LB broth and LB agar, were purchased from Fisher Scientific. All other chemicals were supplied by Sigma-Aldrich Co. and used without further purification.

**Instrumentation.** Absorption spectra were recorded using a Hitachi U-2800 UV−vis−NIR spectrophotometer. Luminescence spectra were recorded using a PTI QuantaMaster spectrofluorometer using 10 mm × 10 mm quartz cuvettes and corrected for detector sensitivity.

Fluorescence lifetime measurements were carried out using a Picoquant FluoTime 200 time correlated single photon counting (TCSPC) setup employing an LDH-P-C-470 ps diode laser (Picoquant) with an excitation wavelength at 466 nm as the excitation source. The laser was controlled by a PDL 800 B picosecond laser driver from Picoquant. $^1$H NMR spectra were recorded on a Bruker AV 400 instrument at 400 MHz. $^{13}$C NMR spectra were recorded on a Varian VNMRS 500 instrument at 125 MHz. ESI mass spectra were measured on a Bruker maXis impact. Laser flash photolysis (LFP) experiments were carried out in a commercially available Luzchem 212 LFP setup provided with a Tektronix TDS 2000 digitizer for signal capture. A Nd:YAG laser (Continuum model Surelite I-10 using second harmonic generators, model number SL-SHG-T1) was used for excitation at a wavelength of 532 nm. Phosphorescence experiments were recorded using a Cary Eclipse fluorescence spectrophotometer. Singlet oxygen phosphorescence was recorded with a Hamamatsu NIR detector (Peltier cooled at −62.8 °C operating at 800 V, coupled to a grating monochromator) upon excitation with a 532 nm Nd:YAG laser. A customized Luzchem Research LFP-111 system was employed to collect and process the data.

## ASSOCIATED CONTENT

### Supporting Information

The Supporting Information is available free of charge on the ACS Publications website at DOI: 10.1021/jacs.5b10288.

Experimental methods, time-resolved absorption, fluorescence, $^1O_2$ phosphorescence studies, phosphorescence of compounds **3**−**6**, biological assays, supporting figures, synthesis of compounds **1**−**8**, and $^1$H NMR and $^{13}$C NMR for compounds **3**−**8** (PDF)

## AUTHOR INFORMATION

### Corresponding Author

*gonzalo.cosa@mcgill.ca

### Notes

The authors declare no competing financial interest.

## ACKNOWLEDGMENTS

G.C. is grateful to the Natural Sciences and Engineering Research Council of Canada (NSERC) and Canada Foundation for Innovation (CFI) for funding. A.M.D. is thankful to the Drug Discovery and Training Program (CIHR) at McGill for a Postdoctoral fellowship. L.E.G. is thankful to Vanier Canada for a postgraduate scholarship, R.L. is thankful to NSERC for a postgraduate scholarship, and S.R.M. acknowledges a DFATD fellowship from Emerging Leaders in the Americas Program (ELAP) to support her visit to Canada and to the Consejo Nacional de Investigaciones Científicas y Técnicas (CONICET) for a research fellowship.

## REFERENCES

(1) Dolmans, D. E.; Fukumura, D.; Jain, R. K. *Nat. Rev. Cancer* **2003**, *3*, 380.
(2) Ogilby, P. R. *Chem. Soc. Rev.* **2010**, *39*, 3181.
(3) Bonnett, R. *Chemical Aspects of Photodynamic Therapy*; CRC Press: Boca Raton, FL, 2000.
(4) Lou, P. J.; Jones, L.; Hopper, C. *Technol. Cancer Res. Treat.* **2003**, *2*, 311.
(5) Bressler, N. M.; Bressler, S. B. *Invest. Ophthalmol. Vis. Sci.* **2000**, *41*, 624.
(6) Agostinis, P.; Berg, K.; Cengel, K. A.; Foster, T. H.; Girotti, A. W.; Gollnick, S. O.; Hahn, S. M.; Hamblin, M. R.; Juzeniene, A.; Kessel, D.; Korbelik, M.; Moan, J.; Mroz, P.; Nowis, D.; Piette, J.; Wilson, B. C.; Golab, J. *Ca-Cancer J. Clin.* **2011**, *61*, 250.
(7) Hamblin, M. R.; Hasan, T. *Photochem. Photobiol. Sci.* **2004**, *3*, 436.
(8) Turro, N. J.; Ramamurthy, V.; Scaiano, J. C. *Modern Molecular Photochemistry of Organic Molecules*; University Science Books: Sausalito, CA, 2012.
(9) Schweitzer, C.; Schmidt, R. *Chem. Rev.* **2003**, *103*, 1685.
(10) Foote, C. S. *Acc. Chem. Res.* **1968**, *1*, 104.


DOI: 10.1021/jacs.5b10288
J. Am. Chem. Soc. 2016, 138, 1215−1225

(11) Zheng, G.; Chen, J.; Stefflova, K.; Jarvi, M.; Li, H.; Wilson, B. C. *Proc. Natl. Acad. Sci. U. S. A.* **2007**, *104*, 8989.
(12) Lovell, J. F.; Liu, T. W.; Chen, J.; Zheng, G. *Chem. Rev.* **2010**, *110*, 2839.
(13) Kamkaew, A.; Lim, S. H.; Lee, H. B.; Kiew, L. V.; Chung, L. Y.; Burgess, K. *Chem. Soc. Rev.* **2013**, *42*, 77.
(14) Huang, L.; Yang, W.; Zhao, J. *J. Org. Chem.* **2014**, *79*, 10240.
(15) Yogo, T.; Urano, Y.; Mizushima, A.; Sunahara, H.; Inoue, T.; Hirose, K.; Iino, M.; Kikuchi, K.; Nagano, T. *Proc. Natl. Acad. Sci. U. S. A.* **2008**, *105*, 28.
(16) Chen, J.; Stefflova, K.; Niedre, M. J.; Wilson, B. C.; Chance, B.; Glickson, J. D.; Zheng, G. *J. Am. Chem. Soc.* **2004**, *126*, 11450.
(17) Trachootham, D.; Zhou, Y.; Zhang, H.; Demizu, Y.; Chen, Z.; Pelicano, H.; Chiao, P. J.; Achanta, G.; Arlinghaus, R. B.; Liu, J.; Huang, P. *Cancer Cell* **2006**, *10*, 241.
(18) Szatrowski, T. P.; Nathan, C. F. *Cancer Res.* **1991**, *51*, 794.
(19) Schumacker, P. T. *Cancer Cell* **2006**, *10*, 175.
(20) Schumacker, P. T. *Cancer Cell* **2015**, *27*, 156.
(21) Gorrini, C.; Harris, I. S.; Mak, T. W. *Nat. Rev. Drug Discovery* **2013**, *12*, 931.
(22) Yogo, T.; Urano, Y.; Ishitsuka, Y.; Maniwa, F.; Nagano, T. *J. Am. Chem. Soc.* **2005**, *127*, 12162.
(23) Kasha, M. *J. Chem. Phys.* **1952**, *20*, 71.
(24) Niki, E.; Noguchi, N. *Acc. Chem. Res.* **2004**, *37*, 45.
(25) Burton, G. W.; Ingold, K. U. *Acc. Chem. Res.* **1986**, *19*, 194.
(26) Khatchadourian, A.; Krumova, K.; Boridy, S.; Ngo, A. T.; Maysinger, D.; Cosa, G. *Biochemistry* **2009**, *48*, 5658.
(27) Krumova, K.; Oleynik, P.; Karam, P.; Cosa, G. *J. Org. Chem.* **2009**, *74*, 3641.
(28) Oleynik, P.; Ishihara, Y.; Cosa, G. *J. Am. Chem. Soc.* **2007**, *129*, 1842.
(29) Krumova, K.; Friedland, S.; Cosa, G. *J. Am. Chem. Soc.* **2012**, *134*, 10102.
(30) Krumova, K.; Greene, L. E.; Cosa, G. *J. Am. Chem. Soc.* **2013**, *135*, 17135.
(31) Lincoln, R.; Greene, L. E.; Krumova, K.; Ding, Z.; Cosa, G. *J. Phys. Chem. A* **2014**, *118*, 10622.
(32) Fragata, M.; Bellemare, F. *Chem. Phys. Lipids* **1980**, *27*, 93.
(33) Fukuzawa, K.; Matsuura, K.; Tokumura, A.; Suzuki, A.; Terao, J. *Free Radical Biol. Med.* **1997**, *22*, 923.
(34) Gorman, A. A.; Gould, I. R.; Hamblett, I.; Standen, M. C. *J. Am. Chem. Soc.* **1984**, *106*, 6956.
(35) Fukuzawa, K.; Inokami, Y.; Tokumura, A.; Terao, J.; Suzuki, A. *Lipids* **1998**, *33*, 751.
(36) Fahrenholtz, S. R.; Doleiden, F. H.; Trozzolo, A. M.; Lamola, A. A. *Photochem. Photobiol.* **1974**, *20*, 505.
(37) Foote, C. S.; Ching, T.-Y.; Geller, G. G. *Photochem. Photobiol.* **1974**, *20*, 511.
(38) Bryan, N.; Ahswin, H.; Smart, N.; Bayon, Y.; Wohlert, S.; Hunt, J. A. *Eur. Cell. Mater.* **2012**, *24*, 249.
(39) auf dem Keller, U.; Kumin, A.; Braun, S.; Werner, S. *J. Invest. Dermatol. Symp. Proc.* **2006**, *11*, 106.
(40) Niethammer, P.; Grabher, C.; Look, A. T.; Mitchison, T. J. *Nature* **2009**, *459*, 996.
(41) Montalban, A. G.; Meunier, H. G.; Ostler, R. B.; Barrett, A. G. M.; Hoffman, B. M.; Rumbles, G. *J. Phys. Chem. A* **1999**, *103*, 4352.
(42) Thapaliya, E. R.; Swaminathan, S.; Captain, B.; Raymo, F. M. *J. Am. Chem. Soc.* **2014**, *136*, 13798.
(43) Gustafson, T. P.; Metzel, G. A.; Kutateladze, A. G. *Photochem. Photobiol. Sci.* **2012**, *11*, 564.
(44) Bartusik, D.; Minnis, M.; Ghosh, G.; Greer, A. *J. Org. Chem.* **2013**, *78*, 8537.
(45) Godin, R.; Liu, H. W.; Smith, L.; Cosa, G. *Langmuir* **2014**, *30*, 11138.
(46) Johnson, I. D.; Kang, H. C.; Haugland, R. P. *Anal. Biochem.* **1991**, *198*, 228.
(47) Bonnett, R. *Chem. Soc. Rev.* **1995**, *24*, 19.
(48) Horrobin, D. F. *New Approaches to Cancer Treatment: Unsaturated Lipids and Photodynamic Therapy*; Churchill Communications Europe: Edinburgh, 1994.
(49) Rapozzi, V.; Miculan, M.; Xodo, L. E. *Cancer Biol. Ther.* **2009**, *8*, 1318.
(50) Loudet, A.; Burgess, K. *Chem. Rev.* **2007**, *107*, 4891.
(51) Wood, T. E.; Thompson, A. *Chem. Rev.* **2007**, *107*, 1831.
(52) Ulrich, G.; Ziessel, R.; Harriman, A. *Angew. Chem., Int. Ed.* **2008**, *47*, 1184.
(53) López Arbeloa, F.; Banuelos, J.; Martinez, V.; Arbeloa, T.; López Arbeloa, I. *Int. Rev. Phys. Chem.* **2005**, *24*, 339.
(54) Krumova, K.; Cosa, G. *J. Am. Chem. Soc.* **2010**, *132*, 17560.
(55) Jiao, L.; Pang, W.; Zhou, J.; Wei, Y.; Mu, X.; Bai, G.; Hao, E. *J. Org. Chem.* **2011**, *76*, 9988.
(56) Krumova, K.; Cosa, G. *Photochemistry: Volume 41* **2013**, *41*, 279.
(57) Yin, H.; Xu, L.; Porter, N. A. *Chem. Rev.* **2011**, *111*, 5944.
(58) Girotti, A. W. *J. Lipid Res.* **1998**, *39*, 1529.
(59) Shahidi, F.; Zhong, Y. *Chem. Soc. Rev.* **2010**, *39*, 4067.
(60) Porter, N. A. *Acc. Chem. Res.* **1986**, *19*, 262.
(61) Lu, Z. T.; Zhang, X. G.; Wu, Z. M.; Zhai, T. T.; Xue, Y. A.; Mei, L.; Li, C. X. *RSC Adv.* **2014**, *4*, 19495.
(62) Ma, J.; Yuan, X. L.; Kucukoz, B.; Li, S. F.; Zhang, C. S.; Majumdar, P.; Karatay, A.; Li, X. H.; Yaglioglu, H. G.; Elmali, A.; Zhao, J. Z.; Hayvali, M. *J. Mater. Chem. C* **2014**, *2*, 3900.
(63) Guo, S.; Ma, L. H.; Zhao, J. Z.; Kucukoz, B.; Karatay, A.; Hayvali, M.; Yaglioglu, H. G.; Elmali, A. *Chem. Sci.* **2014**, *5*, 489.
(64) Lai, Y. C.; Chang, C. C. *J. Mater. Chem. B* **2014**, *2*, 1576.
(65) Adarsh, N.; Avirah, R. R.; Ramaiah, D. *Org. Lett.* **2010**, *12*, 5720.
(66) López Arbeloa, F.; Bañuelos, J.; Martínez, V.; Arbeloa, T.; López Arbeloa, I. *Int. Rev. Phys. Chem.* **2005**, *24*, 339.
(67) Cosa, G.; Scaiano, J. C. *Photochem. Photobiol.* **2004**, *80*, 159.
(68) Galletta, M.; Campagna, S.; Quesada, M.; Ulrich, G.; Ziessel, R. *Chem. Commun. (Cambridge, U. K.)* **2005**, 4222.
(69) Wu, W.; Guo, H.; Wu, W.; Ji, S.; Zhao, J. *J. Org. Chem.* **2011**, *76*, 7056.
(70) Zhang, X. F.; Yang, X. *J. Phys. Chem. B* **2013**, *117*, 5533.
(71) Rehm, D.; Weller, A. *Isr. J. Chem.* **1970**, *8*, 259.
(72) Franco, C.; Olmsted Iii, J. *Talanta* **1990**, *37*, 905.
(73) Wilkinson, F.; Helman, W. P.; Ross, A. B. *J. Phys. Chem. Ref. Data* **1993**, *22*, 113.
(74) Mukai, K.; Daifuku, K.; Okabe, K.; Tanigaki, T.; Inoue, K. *J. Org. Chem.* **1991**, *56*, 4188.
(75) The ratio of physical (95%) to chemical (5%) quenching of $^1O_2$ by PMHC is within experimental error the same for $\alpha$-tocopherol (see ref 34). Both $\alpha$-tocopherol and PMHC have similar overall singlet oxygen quenching rate constant ($k_q = k_{q(physical)} + k_{q(chemical)}$) with values of $2.06 \times 10^8$ $M^{-1}$ $s^{-1}$and $1.96 \times 10^8$ $M^{-1}$ $s^{-1}$, respectively (see ref 74). Our experiments showed that the singlet oxygen quenching rate constant by compound **7** has a value of $2 \times 10^8$ $M^{-1}$ $s^{-1}$. The differences between $\alpha$-tocopherol, PMHC, and our compound rely on their lipophilic tail (phytyl chain, methyl, and BODIPY, respectively, ensuring their partition or lack of within the membrane), yet the chromanol moiety, responsible for the chemical reactivity, is preserved intact in all three compounds ensuring that within error, their chemical and physical quenching constants of $^1O_2$ are the same. We have previously shown, for example, that the chemical reactivity of these compounds with peroxyl radicals (see ref 29) is the same.
(76) Gomes, A.; Fernandes, E.; Lima, J. L. *J. Biochem. Biophys. Methods* **2005**, *65*, 45.
(77) Kinetic competition will determine whether the three control layers may or not be avoided following photoexcitation of **7** to yield $^1O_2$. One may set lower bound values for rate constants of electron transfer in the singlet ($k_{eT}$) and triplet ($k'_{eT}$) manifolds relative to competing processes. Assuming then that in the singlet manifold $k_{eT} \approx 25k_{ISC}$ and that in the triplet manifold $k'_{eT} \approx 10k_q[O_2]$, the fraction of photoexcited **7** effectively sensitizing singlet oxygen is $<4 \times 10^{-3}$. Considering next that geminate (static) quenching of $^1O_2$ by the chromanol trap segment is 100% effective (no escape of $^1O_2$) and that 95−97% of quenching is physical and only 5−3% is chemical


DOI: 10.1021/jacs.5b10288
J. Am. Chem. Soc. 2016, 138, 1215−1225

quenching, then the fraction of photoexcited **7** undergoing activation through reaction with its own singlet oxygen is smaller than $2 \times 10^{-4}$. However $^1O_2$ may escape the solvent cage upon formation ($k_q$ of singlet oxygen is smaller than diffusion control) so it may activate a second molecule of **7** different from the one that generated it.

(78) The sigmoidal curve steepness depends strongly on the parameter *k*, the rate constant for autocatalysis, where a larger *k* determines a steeper curve. The value of the parameter *k* is determined by the combination of a series of rate constants, and among others, it depends directly on the rate of photoexcitation and concentration of $O_2$ (see ref 41).

(79) Dwyer, D. J.; Belenky, P. A.; Yang, J. H.; MacDonald, I. C.; Martell, J. D.; Takahashi, N.; Chan, C. T. Y.; Lobritz, M. A.; Braff, D.; Schwarz, E. G.; Ye, J. D.; Pati, M.; Vercruysse, M.; Ralifo, P. S.; Allison, K. R.; Khalil, A. S.; Ting, A. Y.; Walker, G. C.; Collins, J. J. *Proc. Natl. Acad. Sci. U. S. A.* **2014**, *111*, E2100.

(80) Imlay, J. A.; Chin, S. M.; Linn, S. *Science* **1988**, *240*, 640.



DOI: 10.1021/jacs.5b10288
*J. Am. Chem. Soc.* 2016, 138, 1215−1225